Chemical Engineering Journal 373 (2019) 1179–1189

Contents lists available at ScienceDirect

Chemical Engineering Journal

journal homepage: www.elsevier.com/locate/cej

Unlocking CO_2 separation performance of ionic liquid/CuBTC composites: Combining experiments with molecular simulations

H. Mert Polat[a,c], Muhammad Zeeshan[b,c], Alper Uzun[b,c,d,*], Seda Keskin[b,c,*]

[a] Department of Materials Science and Engineering, Koc University, Rumelifeneri Yolu, 34450 Sariyer, Istanbul, Turkey
[b] Department of Chemical and Biological Engineering, Koc University, Rumelifeneri Yolu, 34450 Sariyer, Istanbul, Turkey
[c] Koc University TUPRAS Energy Center (KUTEM), Koc University, Rumelifeneri Yolu, 34450 Sariyer, Istanbul, Turkey
[d] Koc University Surface Science and Technology Center (KUYTAM), Koc University, Rumelifeneri Yolu, 34450 Sariyer, Istanbul, Turkey

HIGHLIGHTS

- A computational method was proposed to predict gas uptakes of IL/CuBTC composites.
- Molecular simulations accurately predicted gas uptakes of two new composites.
- IL/CuBTC composites have higher CO_2 selectivities than the pristine CuBTC.

ARTICLE INFO

Keywords:
Ionic liquid (IL)
Metal organic framework (MOF)
Molecular simulations
Gas separation
Carbon dioxide (CO_2)

ABSTRACT

In this work, we propose a computational methodology based on the state-of-the-art molecular simulations of IL/CuBTC composites composed of ILs having the same cation, 1-*n*-butyl-3-methylimidazolium ($[BMIM]^+$), and various anions. Using grand canonical Monte Carlo (GCMC) simulations, we predicted CO_2, CH_4, and N_2 uptakes of seven different IL/CuBTC composites and compared the simulation results with our experimental gas uptake measurements to select the most appropriate force field that best represents the experimental results. Motivated from the good agreement between experiments and simulations, we applied the same method to estimate the gas adsorption in two new IL/CuBTC composites which have been synthesized and characterized for the first time in this work. Molecular simulations accurately predicted the experimental gas uptakes of newly synthesized IL/CuBTC composites, validating the transferability of our approach to different types of IL-incorporated CuBTC samples. We also provided a detailed analysis of binary gas mixture separation performances of IL/CuBTC composites and self-diffusion coefficients of gases in the composites performing GCMC and molecular dynamics simulations, respectively. Results showed that IL/CuBTC composites have higher CO_2/CH_4, CO_2/N_2, and CH_4/N_2 selectivities than those of CuBTC, demonstrating a broad potential of these composites for CO_2 separation from natural gas and flue gas mixtures. The combination of experiments and molecular simulations that we described in this study will be useful to efficiently screen various IL/MOF composites to unlock their full potential for gas separation applications.

1. Introduction

Carbon dioxide (CO_2) capture from natural gas and flue gas has a significant environmental, social, economic, and industrial importance [1–3]. CO_2 concentration in the atmosphere increased from 280 ppm in the pre-industrial revolution time to above 400 ppm today [4]. Contribution of emissions from fossil fuels to this increase is higher than 2 ppm per year, presenting the importance of CO_2 capture from flue gas [5]. On the other hand, presence of CO_2 in the natural gas decreases its energy density and causes corrosion in pipelines. Although the limit of CO_2 concentration in the natural gas is dictated by different regulations, it is generally expected not to exceed 2% [6]. Therefore, developing efficient technologies for CO_2 separation from flue gas and natural gas has significant environmental importance. Among many available techniques [7], adsorption-based CO_2 separation is widely preferred since it is low-cost, efficient, and easy to operate. A large variety of porous materials have been developed and tested for adsorption-based CO_2 separation to date, including activated carbons [8], zeolites [9],

* Corresponding authors at: Department of Chemical and Biological Engineering, Koc University, Rumelifeneri Yolu, 34450 Sariyer, Istanbul, Turkey.
E-mail addresses: auzun@ku.edu.tr (A. Uzun), skeskin@ku.edu.tr (S. Keskin).

https://doi.org/10.1016/j.cej.2019.05.113
Received 20 February 2019; Received in revised form 15 May 2019; Accepted 18 May 2019
Available online 20 May 2019
1385-8947/ © 2019 The Authors. Published by Elsevier B.V. This is an open access article under the CC BY license (http://creativecommons.org/licenses/BY/4.0/).

silica gels [10], carbon nanotubes [11], and metal organic frameworks (MOFs) [12,13].

MOFs are a relatively new group of crystalline porous materials comprised of metal ions or clusters connected to each other with organic linkers [14]. They have gained significant attention because of their extraordinary properties, such as very high surface areas, high porosities, low densities, and tunable structures [15], which make them potential materials in various applications including catalysis [16], drug delivery [17], fuel cell applications [18], gas storage, and gas separation [13,19]. MOFs have been considered as strong candidates for gas adsorption and various gas separation applications, because they can be designed with desired structural and chemical properties for a target process [20–22]. However, complicated synthesis procedures are often required to discover new MOFs having high gas separation performances. Post-synthesis modification of MOFs creates an alternative to this approach offering materials having high performance with relatively simpler synthesis procedures. A very recent approach is the post-synthesis modification of MOFs with ionic liquids (ILs) to tune the gas adsorption and selectivity of MOFs. ILs, organic salts that are liquid below 100 °C [23], have high thermal stabilities, negligible vapor pressures, and ionic conductivities [24,25]. Similar to MOFs, practically infinite number of ILs can be synthesized by changing the combinations of cations and anions. Thanks to their tunable properties, ILs have been widely utilized in synthesis [26,27], catalysis [28,29], and gas absorption and separation [30,31]. Recent studies have focused on incorporation of ILs into MOFs [32] or coating the external surface areas of MOFs with ILs to make IL/MOF composites [33], which offer significantly improved gas adsorption and/or separation performance compared to that of the host MOF.

IL/MOF composites are a new type of composite materials which are used for various applications [34,35], mainly for adsorption-based CO_2 separation [32,33,36,37]. Combining the high porosity and the high surface area of MOFs with high gas solubility of ILs, these composites offer a great potential for efficient gas storage and gas separation [38]. However, it is not possible to experimentally synthesize and test every single IL/MOF composite for a desired application, because of the infinite number of possible IL/MOF pairs. Molecular simulations have been very useful to screen large numbers of materials and to identify the best ones for a target application. They have been widely used to accurately predict gas storage and separation performances of MOFs [39,40]. Similarly, molecular simulation methods have been used for screening ILs for absorption-based gas separations [41]. However, there are only a handful of molecular simulation studies that investigated IL/MOF composites for gas storage and separation as we briefly discuss below.

Chen et al. [42] performed a molecular simulation study for an IL/MOF composite, [BMIM][PF_6]/IRMOF-1, and showed that the composite is more selective for CO_2 over N_2 than the pristine IRMOF-1 using grand canonical Monte Carlo (GCMC) simulations. Vicent-Luna et al. [43] used GCMC simulations to show that incorporation of ILs significantly increases the CO_2 uptake of CuBTC at low pressures, whereas changes in CH_4 and N_2 uptakes are negligible. Li et al. [44] performed GCMC simulations and showed that IL impregnation into Cu-TDPAT increases the selectivity of H_2S over CH_4 with increasing IL loading. Xue et al. [45] investigated both IL/MOF and IL/covalent organic frameworks (COFs) composites using GCMC and molecular dynamics (MD) simulations and reported that better IL dispersion inside the pores results in better selectivity of CO_2 over CH_4 and N_2. Vicent-Luna et al. [46] showed that small additions of ILs into COFs significantly increase their CO_2/CH_4 selectivity compared to the hydrated COFs. The same group [47] also examined [EMIM][SCN] incorporated IRMOF-1, HMOF-1, MIL-47, and MOF-1 using density functional theory (DFT) calculations, GCMC, and MD simulations; and reported that CO_2/CH_4, CO_2/N_2, and CH_4/N_2 selectivities of the composites increase with increasing IL loading. Gupta et al. [48] studied four different IL-incorporated IRMOF-1 composites for membrane-based separation of CO_2 from flue gas using MD simulations and showed that [BMIM][SCN]/IRMOF-1 membrane can surpass the Robeson's upper bound. They also investigated [BMIM][SCN]/ZIF-71 and [BMIM][SCN]/ZMOF composites using MD simulations and concluded that CO_2/N_2 selectivity of the composite in membrane-based separation is dominated by the adsorption selectivity [49]. All these computational studies have been very useful to predict the gas adsorption and gas separation performances of several different IL/MOF composites; however, none of these studies, to the best of our knowledge, included experimentally measured gas adsorption data of the composites to compare with the simulation results.

We recently combined experiments and molecular simulations for an IL/MOF composite and presented the good agreement between experimental measurements and predictions of GCMC simulations for single-component adsorption isotherms of CO_2, CH_4, and N_2 in a [BMIM][PF_6]/ZIF-8 composite [32]. It was shown that IL/ZIF-8 composite more than doubles the CO_2/CH_4 and CO_2/N_2 selectivities of pristine ZIF-8 at low pressures. A follow-up study combining experimental and computational work [36] focused on [BMIM][BF_4]/ZIF-8 composite and presented the good agreement between experiments and molecular simulations for the heat of adsorption values for CO_2, CH_4, and N_2 in the composite. The work also showed that CO_2/CH_4, CO_2/N_2, and CH_4/N_2 selectivities enhance at low pressures upon IL incorporation into ZIF-8. These combined experimental and computational studies only investigated two types of IL/MOF composites having the same MOF, ZIF-8. In order to have a comprehensive understanding of IL/MOF composites, various types of materials should be investigated so that molecular simulations can be validated by comparing with the experiments and then these molecular simulations can be used for high-throughput screening of new IL/MOF composites for which the experimental data are not available. In this way, IL/MOF composites that offer high selectivities for gas separations can be accurately and effectively identified by molecular simulations and then the experimental efforts, time, and resources can be directed towards the investigation of these most promising materials.

Motivated from this idea, we performed GCMC simulations to predict CO_2, CH_4, and N_2 adsorption in seven different IL/CuBTC composites consisting of ILs with the $[BMIM]^+$ cation and a commonly used, commercial MOF, CuBTC. We compared simulation results with the experimental gas uptake measurements of these composites to propose a computational screening approach that is applicable to various IL/CuBTC composites. This approach was then tested on two new IL/CuBTC composites which have not been synthesized before to unlock their gas adsorption and separation performances. We showed the transferability of our computational methodology to these two new IL/CuBTC composites by synthesizing and characterizing them and comparing the experimentally measured gas adsorption data with the simulations. To the best of our knowledge, this is the first study that proposes a computational methodology for high-throughput screening of IL/CuBTC composites and that confirms the validity of this methodology experimentally on new composites, presenting a broad potential for being expanded to other types of ILs and MOFs in the future.

2. Methods

2.1. Computational methods

We studied a total of nine different ILs in this work: 1-*n*-butyl-3-methylimidazolium tetrafluoroborate ([BMIM][BF_4]), 1-*n*-butyl-3-methylimidazolium trifluoromethanesulfonate ([BMIM][CF_3SO_3]), 1-*n*-butyl-3-methylimidazolium methylsulfate ([BMIM][$MeSO_4$]), 1-*n*-butyl-3-methylimidazolium methanesulfonate ([BMIM][$MeSO_3$]), 1-*n*-butyl-3-methylimidazolium hexafluorophosphate ([BMIM][PF_6]), 1-*n*-butyl-3-methylimidazolium hexafluoroantimonate ([BMIM][SbF_6]), 1-*n*-butyl-3-methylimidazolium octylsulfate ([BMIM][$OcSO_4$]), 1-*n*-butyl-3-methylimidazolium dicyanamide ([BMIM][DCA]), and 1-*n*-butyl-3-methylimidazolium dibutylphosphate ([BMIM][DBP]). Molecular

structures of ILs and CuBTC are shown in Fig. S1 of Supplementary Materials (SM). The IL structures were optimized by using Gaussian 09 software [50]. Conformer search was done to obtain the energetically the most stable structures of the cation and the anions. The cation ($[BMIM]^+$) and the anions ($[BF_4]^-$, $[CF_3SO_3]^-$, $[MeSO_4]^-$, $[MeSO_3]^-$, $[PF_6]^-$, $[OcSO_4]^-$, $[DCA]^-$, and $[DBP]^-$) were optimized using the Becke's three parameter hybrid exchange functional [51] and the Lee-Yang-Parr correlation functional [52] (B3LYP) and by using the 6-31 + G(d) basis set. $[SbF_6]^-$ anion was optimized using the density Gauss double-zeta with polarization functions (DGDZVP) basis set [53]. In these calculations, the convergence was set to tight criteria (10^{-8} on root-mean-square density matrix, 10^{-6} on maximum density matrix, and 10^{-6} on maximum energy). To find the energetically most stable structures, conformer search was performed for the anion-cation pairs by using the same parameters given above and considering different anion orientations around the cation. The most stable conformer for ILs, except for $[BMIM][SbF_6]$, was then further optimized by using 6-311 + G(2d,p) basis set to increase the calculation accuracy. Population analyses were carried out to calculate the partial charges using full Natural Bond Orbital (NBO) analysis with NBO version 3.1 [54,55]. Optimized IL structures were then used in the GCMC and MD simulations of IL/MOF composites.

All GCMC and MD simulations were performed using the RASPA software [56]. Molecular simulations were performed twice using two different generic force fields, Universal Force Field (UFF) [57] and Dreiding [58], for both CuBTC and IL/CuBTC composites. For Cu atoms, the potential parameters were taken from the UFF since they are not available in the Dreiding. After comparing the predictions of simulations and experimental results, the force field that best represents the experimental gas uptake data of the composites was selected. Force field parameters used in molecular simulations can be found in Table S1 of SM.

CO_2 was modeled using a three-site rigid model with Lennard-Jones (LJ) 12-6 potential, where locations of point charges were the center of each site [59]. CH_4 was modeled as a spherical single-site LJ 12-6 potential [60]. N_2 was modeled as a three-site molecule, where two sites were N atoms and the third one was at the center of mass with point charges [61]. Parameters used for gas molecules in molecular simulations are given in Table S2. Cross-atomic force field parameters were calculated using the Lorentz-Berthelot mixing rules and intermolecular interactions were truncated at 12 Å. CuBTC and ILs were considered as rigid structures during the simulations to save significant computational time. Since adsorbate molecules are relatively small compared to the pore size of CuBTC and IL/CuBTC composites as shown in Table S3, flexibility is expected to have a negligible effect on the simulated gas uptakes as previously shown in the literature [62]. The largest cavity diameters (LCDs) and pore limiting diameters (PLDs) of pristine CuBTC and IL/CuBTC composites were calculated using Zeo + + software [63]. The Baker minimization method with NVT ensemble was used to incorporate ILs into CuBTC, as implemented in the RASPA. In this method, a minimum energy configuration with all positive eigenvalues in Hessian matrix was obtained [64]. We calculated the required number of IL molecules that will lead to 30 wt% IL-loading in the composite to be consistent with the previous experimental works [65–67] using the weight of one unit cell of CuBTC and molar weight of ILs. An IL loading of 30 wt% was reported to provide the highest selectivity of the composites without forming a muddy product as discussed in our previous work [65]. It should be noted that there may be deviations between the pre-determined IL loading (30 wt%) and the actual loading reported in the experimental studies because some part of the IL may be lost on the glass container that is used for the preparation of composites [32]. The number of IL molecules incorporated into CuBTC and calculated IL loading for each composite are given in Table S4. ILs were inserted inside CuBTC using three different GCMC moves, translation, rotation, and random translation. The energy minimization procedure was continued until the root-mean-square gradient and maximum gradient were smaller than 10^{-6}. In these simulations, crystal structure of CuBTC and its partial charges were taken from the RASPA [56]. For ILs, point charges computed by DFT calculations were used. Both the atomic positions and point charges of ILs are given in Tables S6–S14 of SI. Since incorporation of ILs into CuBTC changes the electronic environment [32,36,65], we reassigned the partial charges of IL/MOF structures using the charge equilibration (QEq) [68] method as implemented in the RASPA and computed the electrostatic interactions between adsorbates having quadrupole moments (CO_2, N_2) and the atoms of IL/MOF composites.

Single-component and binary mixture gas adsorption simulations of IL/MOF composites were performed in a pressure range of 0.1–10 bar at 25 °C. These simulations were carried out for 5×10^4 cycles for initialization and 5×10^5 cycles for taking the ensemble averages. In single-component GCMC simulations, four different types of moves, translation, rotation, reinsertion, and swap, were used. For the binary mixture GCMC simulations, an additional move, the identity exchange was also considered. The compositions of the mixtures were set as CO_2/CH_4:50/50, CO_2/N_2:15/85, and CH_4/N_2:50/50 to mimic the flue gas and natural gas separations. The Peng-Robinson equation of state was used to convert the pressure to fugacity. Pore volumes and void fractions of IL/CuBTC composites were calculated by using Zeo + + [63] using a probe diameter of 0 Å and calculated void fractions were used in the GCMC simulations to convert the absolute gas uptakes to excess values to compare the results of simulations with those of the experiments. The experimental results of gas uptake measurements on $[BMIM][BF_4]$/CuBTC, $[BMIM][CF_3SO_3]$/CuBTC, $[BMIM][MeSO_4]$/CuBTC, $[BMIM][MeSO_3]$/CuBTC, $[BMIM][SbF_6]$/CuBTC, $[BMIM][PF_6]$/CuBTC, and $[BMIM][OcSO_4]$/CuBTC composites were taken from our previous publications [65–67]. We note that our previous article [67] on $[BMIM][PF_6]$/CuBTC reported CO_2, CH_4, and N_2 uptakes from 0.1 to 1 bar; however, here, we present the gas uptakes from 0.1 to 10 bar for the same composite. Values of coefficient of determinations (R^2) were calculated using, $R^2 = 1 - \frac{\sum_0^{n-1}(y_i - \hat{y}_i)^2}{\sum_0^{n-1}(y_i - \bar{y})^2}$, where y_i is the experimental value, $\hat{y}_i$ is the prediction from simulations, $\bar{y}$ is the arithmetic average of all experimental values and n is the number of data points to quantify the goodness of prediction of simulations compared to the experimental data.

Finally, MD simulations within NVT ensemble using Nose-Hoover thermostat [69,70] were performed to calculate the single-component self-diffusivity coefficient (D^0) of CO_2, CH_4, and N_2 in IL/CuBTC composites at infinite dilution. Gas-gas intermolecular interactions were switched-off to mimic the infinite dilution condition and 30 gas molecules were added inside the IL/CuBTC composites. MD simulations were performed by turning-off these interactions alternately to isolate the contributions of IL-gas and CuBTC-gas interactions. 1000 initialization and 10,000 equilibration cycles were performed at the start of each simulation. MD simulations were performed for a total of 5 ns using a time step of 0.5 ps. Self-diffusion coefficients of gases were calculated from the slope of mean square displacement of the gas molecules obtained from the MD simulations.

2.2. Experimental methods

2.2.1. Sample preparation

In this work, two new IL/CuBTC composites, [BMIM][DCA]/CuBTC and [BMIM][DBP]/CuBTC, which have not been reported in the literature before, were synthesized. [BMIM][DCA] (> 97%, Sigma Aldrich), [BMIM][DBP] (> 96%, Sigma Aldrich) and CuBTC (Basolite C300, Sigma Aldrich) were purchased from Sigma Aldrich. ILs and CuBTC were stored in an Ar (> 99.999%, Linde) glovebox (Labconco). We dried the ILs at 80 °C for 6 h and kept them under vacuum for 12 h before transferring them into the glovebox [71]. CuBTC was activated overnight at 105 °C under vacuum before usage. To prepare the samples with 30 wt% IL loading, 0.3 g of [BMIM][DCA] or [BMIM][DBP] was

dissolved in 20 mL of acetone (> 99.8%, Merck) for 1 h. 0.7 g of CuBTC was then added into the solution and acetone was evaporated from the solution at 35 °C under atmospheric conditions. Muddy product from mostly evaporated solution was completely dried in the oven at 105 °C. Final product was stored in a desiccator until further usage.

2.2.2. Sample characterization

2.2.2.1. X-ray diffraction (XRD). The XRD patterns of pristine CuBTC, [BMIM][DCA]/CuBTC, and [BMIM][DBP]/CuBTC were obtained by a Bruker D8 Advance X-ray Diffractometer using a Lynxeye detector equipped with a slit of 1 mm. X-ray generator was set to 30 kV voltage and 10 mA current producing Cu $K\alpha_1$ (1.5406 Å) radiation. The diffraction patterns were obtained between 2θ values of 5-50° with a resolution of 0.0204°.

2.2.2.2. Scanning electron microscopy (SEM). SEM imaging was done using a Zeiss Ultra Plus Field Emission SEM (FESEM) with an accelerating voltage of 3 kV and working distance of approximately 4 mm. Materials were placed on a carbon tape attached on pin mount sample holder and coated with carbon to prevent charging during imaging.

2.2.2.3. Fourier transform infrared (FTIR) spectroscopy. The infrared spectrum of CuBTC, [BMIM][DCA]/CuBTC, [BMIM][DBP]/CuBTC, and bulk ILs were obtained by using a Thermo Scientific Nicolet iS50 FTIR spectrometer equipped with an attenuated total reflection (ATR) cell. For background and sample, 64 and 512 scans were collected, respectively. The FTIR spectra of samples were collected between 400 and 4000 cm^{-1} with a spectral resolution of 2 cm^{-1}.

2.2.2.4. Brunauer-Emmett-Teller (BET) surface area. BET analyses were performed by using a Micromeritics ASAP 2020 physisorption analyzer. Approximately 200 mg of sample was used. Materials were activated at 125 °C under vacuum, then the samples were cooled down to −196 °C using liquid nitrogen before the analyses. The free space measurements were conducted using helium gas. N_2 gas adsorption isotherms of materials were obtained at −196 °C between 10^{-6} and 1 bar.

2.2.2.5. Thermogravimetric analysis (TGA). A TA Instruments Q500 thermogravimetric analyzer was used to determine the thermal stability limits of pristine CuBTC, [BMIM][DCA]/CuBTC, [BMIM][DBP]/CuBTC, and bulk ILs. An empty platinum pan was tared and approximately 15 mg of sample was placed on it. Then, a temperature ramp of 5 °C/min was applied until the temperature reached 125 °C. An isothermal treatment at 125 °C for 8 h was conducted to remove any moisture from the samples. After that, a temperature ramp of 2 °C/min was applied up to 700 °C. N_2 was used as balance and purge gas with flow rates of 40 and 60 mL/min, respectively. From the thermogravimetry (TG) and derivative TG curves, onset (T_{onset}) and derivative onset (T_{onset}') temperatures obtained. T_{onset} generally overestimates the decomposition temperature, thus T_{onset}' was considered as decomposition temperature in this study [32].

2.2.3. Gas adsorption measurements

CO_2, CH_4, and N_2 adsorption isotherms of pristine CuBTC, [BMIM][DCA]/CuBTC, and [BMIM][DBP]/CuBTC were obtained using a Micromeritics High Pressure Volumetric Analyzer II (HPVA-II-200). Before the measurements, approximately 350 mg of sample was activated at 125 °C under vacuum until the pressure inside the sample holder reaches to 10^{-6} bar. Then, the system was purged with He for three-times to eliminate the impurities and residuals from previous measurements. Temperature was set to 25 °C and held constant throughout the measurements, while the temperature of the laboratory was maintained at 23 °C. Gas adsorption isotherms were obtained in a pressure range of 0.1–10 bar.

3. Results and discussion

3.1. Force field selection for molecular simulations of IL/CuBTC composites

Adsorption of CO_2, CH_4, and N_2 in CuBTC has been widely studied in the literature using molecular simulations employing different force fields by several research groups [72–76]. We performed GCMC simulations using two different generic force fields, UFF and Dreiding, to examine which force field provides a better representation of the experimental gas adsorption data in CuBTC. Fig. 1(a) compares our experimental results of CO_2, CH_4, and N_2 uptakes in CuBTC with the predictions of GCMC simulations using UFF and Dreiding at a pressure range of 0.1–10 bar at room temperature. Based on the data presented in Fig. 1, both force fields overestimated CO_2 and N_2 uptakes, whereas CH_4 uptakes were underestimated. For all gases at all pressures, predictions of UFF were found to be slightly higher than those of Dreiding. Fig. 1(b) compares the experimental and simulated gas uptakes and the inset table shows the goodness of the agreement between them as quantified by the R^2 values. R^2 values were computed to be > 0.9 for all gases except for N_2 when Dreiding force field was used. Once the

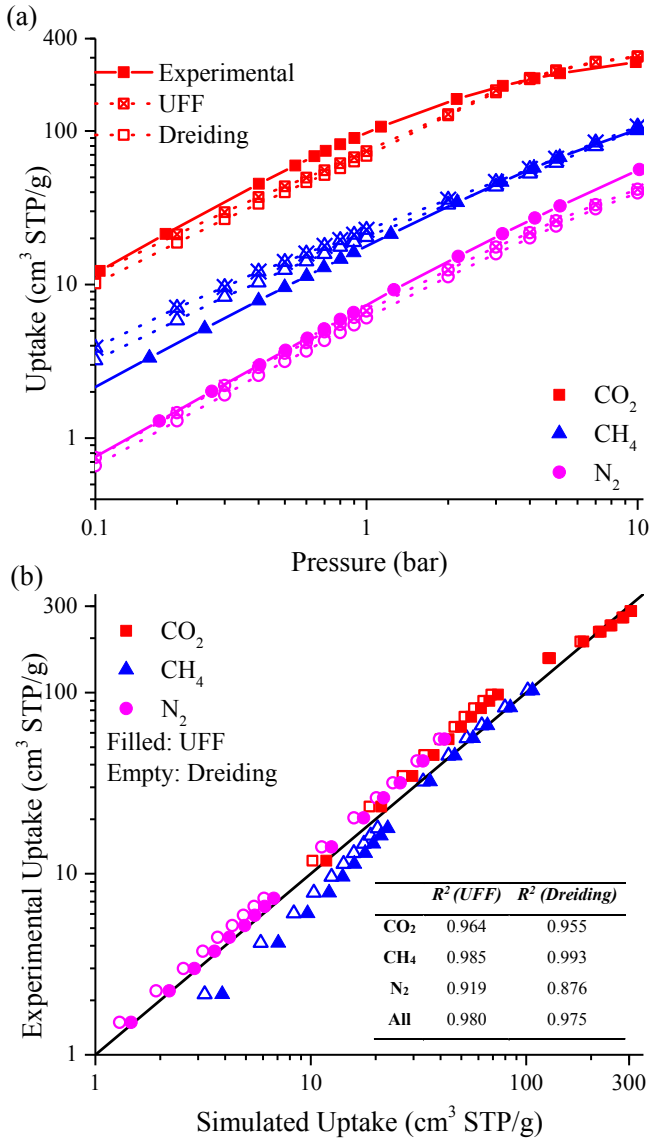


Fig. 1. (a) Single-component adsorption isotherms of CO_2, CH_4, and N_2 as a function of pressure in pristine CuBTC, (b) comparison of experiments and simulations using UFF and Dreiding force fields for CuBTC.

overall prediction performances of the two force fields were considered for three gases at 16 different pressure points, R^2 values were computed as 0.980 for UFF and 0.975 for Dreiding, respectively, indicating that both generic force fields can be used to accurately estimate CO_2, CH_4, and N_2 uptakes of pristine CuBTC, which is consistent with the literature [43,76].

After we validated the accuracy of molecular simulations for predicting CO_2, CH_4, and N_2 uptakes of pristine CuBTC, we applied the same computational approach to IL/CuBTC composites. We studied seven different IL/CuBTC composites, for which our group already has the experimental gas adsorption data for CO_2, CH_4, and N_2, as reported in our previous reports [65–67]. These IL/CuBTC composites are [BMIM][BF_4]/CuBTC, [BMIM][CF_3SO_3]/CuBTC, [BMIM][$MeSO_4$]/CuBTC, [BMIM][$MeSO_3$]/CuBTC, [BMIM][SbF_6]/CuBTC, [BMIM][PF_6]/CuBTC, and [BMIM][$OcSO_4$]/CuBTC. We performed molecular simulations for these composites and predicted their CO_2, CH_4, and N_2 uptakes between 0.1 and 10 bar at 25 °C. These GCMC simulations were performed by using both UFF and Dreiding to investigate which force field provides a better prediction for the gas uptake performances of the corresponding IL/CuBTC composite. Comparison of simulation results with the experimental gas uptake measurements are shown in Fig. 2. Results indicate that simulations employing either of the force fields generally overestimate the experimental gas uptake values of all IL/CuBTC composites. Simulations using Dreiding force field tend to give a better agreement with the experiments than the ones using UFF. R^2 values were computed as 0.840, 0.734, and 0.913 for CO_2, CH_4, and N_2, respectively, when Dreiding was used in the molecular simulations, whereas UFF was found to result in much lower R^2 values (< 0.6) for all gases. Overall, Fig. 2 suggests that molecular simulations using Dreiding force field can provide reasonably accurate predictions for adsorption of CO_2, CH_4, and N_2 in these seven different IL/CuBTC composites at a wide pressure range.

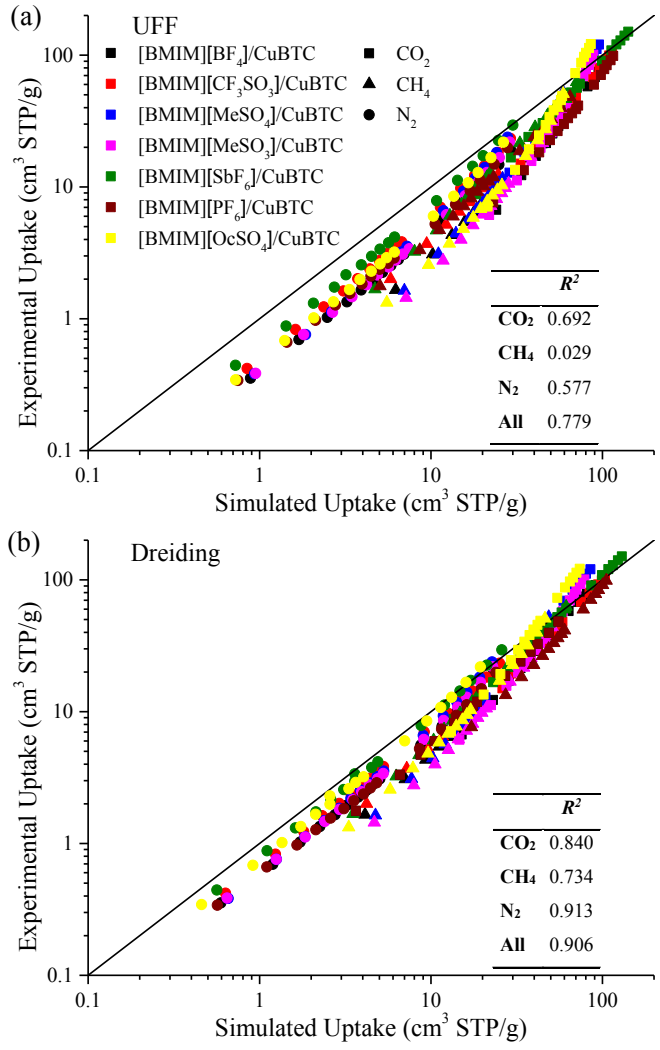


Fig. 2. Comparison of experiments with simulations using (a) UFF and (b) Dreiding force fields for gas uptakes in seven different IL/CuBTC composites.

Correcting simulation results using a scaling factor has been previously done in several molecular simulation studies [77–82] to compensate the slight systematic deviations between experiments and simulations, which generally results from the possible crystal defects, residual solvents, inaccessible adsorption sites of MOFs, or some specific interactions between MOFs and adsorbates that are not well-represented by the generic force fields [78,82–84]. Thus, to improve the agreement between simulations and experiments, uptakes obtained from GCMC simulations were multiplied by a pressure dependent factor (s_i) as follows, $s_i = A_i \times (\log(P) + 2)$, where P is the pressure and A_i is the coefficient of scaling function changing with pressure range (defined for low pressure (< 0.3 bar), moderate pressure (0.3–1 bar) and high pressure (> 1 bar) regions) and gas species. The constant "2" was added to this factor to eliminate the possibility of zero multipliers at 0.1 and 1 bar pressures. We note that scaling factors do not have specific physical meanings, they were purely defined by fitting the simulation results to experiments. Table S15 lists the scaling factors that we defined for each of the pressure region, low, moderate, and high pressure. The data of Fig. 2 show that deviations between the experiments and simulations are much higher at lower pressures compared to the ones at higher pressures. As a result of this, the coefficients of the scaling function (A_i) show a decreasing trend with increasing pressure for all adsorbates (Table S15).

Fig. 3 compares the experimental gas uptakes of IL/MOF composites with the scaled simulations, which are in a much better agreement with the experimental data compared to the non-scaled ones. The inset table in Fig. 3(d) shows the R^2 values for the scaled simulation results. Accordingly, the R^2 values increased from 0.840 to 0.904 for CO_2, from 0.734 to 0.972 for CH_4, and from 0.913 to 0.970 for N_2 uptakes of seven different IL/MOF composites. The better agreement of simulations with experiments after scaling indicates that ideal selectivities, which were calculated as the ratio of single-component gas uptakes, can also be well-predicted by the simulations. Comparison of experimental and simulated ideal selectivities for CO_2/CH_4, CO_2/N_2, and CH_4/N_2 shown in Fig. S2 present the good agreement between two. Overall, we showed that molecular simulations using Dreiding force field and the function that we introduced above to scale the simulated gas uptakes can be used to accurately estimate the gas uptake and separation performances of IL/CuBTC composites, where ILs are composed of $[BMIM]^+$ cation and different types of anions, which are not too big in size not to limit their transport into the pores.

3.2. Application of computational approach to two different IL/CuBTC composites

The computational approach that we described above was developed and validated by using seven different IL/CuBTC composites for which our group already had the experimental gas adsorption data. Next, we performed GCMC simulations of CO_2, CH_4, and N_2 adsorptions on two new composites, [BMIM][DCA]/CuBTC and [BMIM][DBP]/CuBTC, to confirm the transferability of this approach to other IL/CuBTC composites. We note that these two composites have not been reported before in the literature. These two ILs were chosen as they are commonly available and we also aimed to select the anions of ILs in a way to represent a small ($[DCA]^-$) and a large anion ($[DBP]^-$). This approach let us to test the transferability of our computational approach to predict gas uptakes and selectivities of different IL/CuBTC composites, where ILs are composed of the same $[BMIM]^+$ cation with

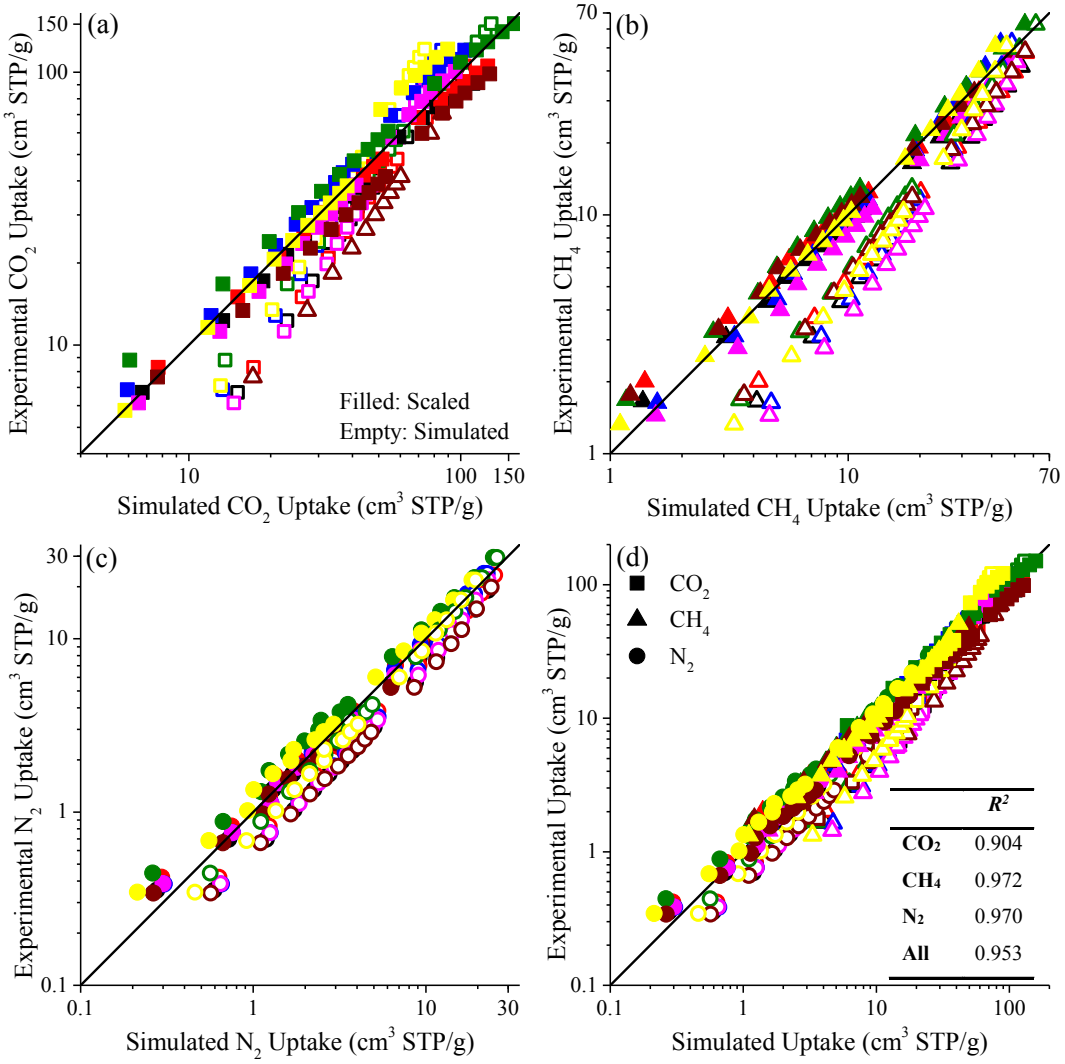


Fig. 3. Comparison of scaled and unscaled simulations with experimental uptakes of (a) CO_2, (b) CH_4, (c) N_2, and (d) all gases. Filled (empty) symbols represent scaled (non-scaled) simulations. Color code follows that in Fig. 2.

different anions. We synthesized and characterized these two new composites and measured their gas uptake performances. Before focusing on the simulation results, we first discuss the characterization of these two new composites. Fig. 4(a) illustrates the XRD diffraction patterns of pristine CuBTC, [BMIM][DCA]/CuBTC, and [BMIM][DBP]/CuBTC composites. These results show that crystal structure of CuBTC was preserved upon IL incorporation. SEM images shown in Fig. S3 confirm that crystal size and shape do not change in the composite materials when compared with those of CuBTC. Fig. 4(b) shows thermogravimetric curves of pristine CuBTC and the new composites. More detailed comparisons of TGA results of composites with their respective bulk ILs and pristine CuBTC are given in Figs. S4 and S5. The derivative onset temperature (T_{onset}') of pristine CuBTC was found as 324 °C. T_{onset}' of [BMIM][DCA]/CuBTC and [BMIM][DBP]/CuBTC were found as 254 °C and 178 °C, while bulk ILs, [BMIM][DCA] and [BMIM][DBP], were found to start to decompose at 226 °C and 228 °C, respectively. These changes in T_{onset}' values indicate the presence of direct interactions between CuBTC and ILs, which might be because of the slight structural alterations in the individual components of the composite. FTIR spectra of pristine CuBTC, bulk ILs, and composites are shown in Fig. 4(c). Three intense peaks between 2100 and 2300 cm^{-1} in the spectrum of bulk [BMIM][DCA] were assigned to asymmetric stretching of −C≡N group (ν_{as}(−C≡N)), symmetric stretching of −C≡N group (ν_s(−C≡N)) and combination of these two modes [85]. In [BMIM][DCA]/CuBTC composite, ν_{as}(−C≡N) shifted from 2126 cm^{-1} to 2165 cm^{-1}, ν_s(−C≡N) shifted from 2191 cm^{-1} to 2212 cm^{-1} and the combination of these two modes shifted from 2229 cm^{-1} to 2285 cm^{-1}. Symmetric stretching deformation of second carbon of the imidazolium group and the proton bonded to it (ν_s(−C2H)) exhibited a red shift from 3101 cm^{-1} to 3086 cm^{-1}. Similar shifts in the position of bands were also seen in [BMIM][DBP]/CuBTC composite. After IL-incorporation, −P═O stretching vibration [86] (ν_s(−P═O)) at 1233 cm^{-1} and ν_s(−C2H) at 3097 cm^{-1} shifted to 1239 cm^{-1} and 3093 cm^{-1}, respectively. These shifts in the positions of characteristic bands of ILs confirm the presence of direct interactions between CuBTC and incorporated ILs. Next, we washed the [BMIM][DCA]/CuBTC and [BMIM][DBP]/CuBTC composites with toluene to validate that the ILs were successfully incorporated into the pores of CuBTC. We chose toluene as it is larger than the pore openings of CuBTC so it cannot go into the pores yet it is capable of dissolving both of these ILs at room temperature [67]. Fig. S6 shows the FTIR spectra of toluene, the filtrates of washing process, and the corresponding composites before and after washing. Data showed that the spectra of the filtrates did not have any evident IL bands, while the spectra of the composites were showing the characteristic IL bands still present in the composites even after the washing experiment. These results confirmed that the incorporation of ILs into the pores was successful for both composites. Fig. S7 also shows that N_2 adsorption at −196 °C is quite different for two composites although

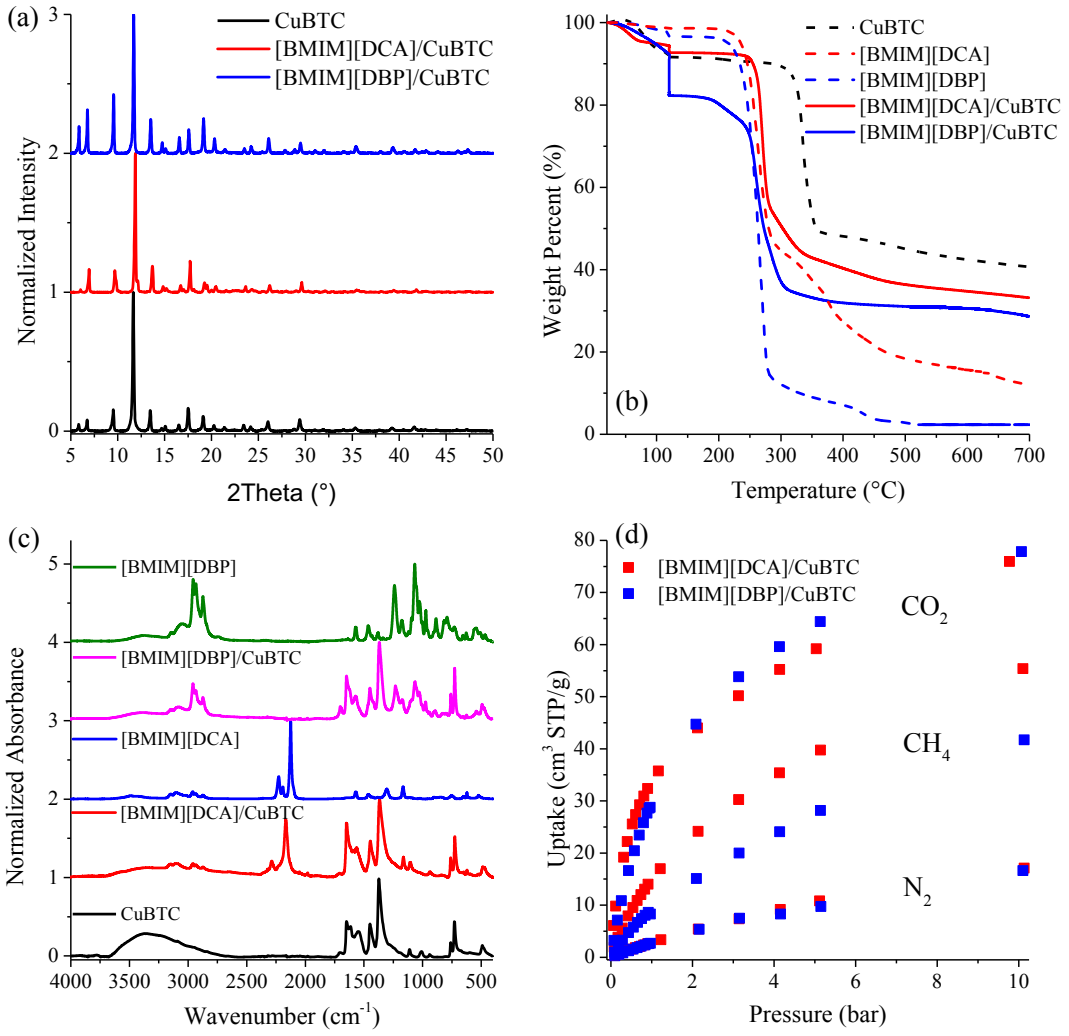


Fig. 4. (a) XRD patterns, (b) TGA curves of CuBTC, [BMIM][DCA]/CuBTC, [BMIM][DBP]/CuBTC, and bulk ILs, (c) FTIR spectra of CuBTC, [BMIM][DCA]/CuBTC, [BMIM][DBP]/CuBTC, and bulk ILs, (d) CO_2, CH_4, and N_2 adsorption isotherms of [BMIM][DCA]/CuBTC and [BMIM][DBP]/CuBTC.

their CO_2, CH_4, and N_2 adsorption isotherms at room temperature are similar (Fig. 4(d)), which may be attributed to the low solubility of N_2 in ILs at −196 °C rendering the BET method unreliable for this type of materials [66]. Fig. 4(d) shows the experimental adsorption isotherms of CO_2, CH_4, and N_2 between 0.1 and 10 bar for [BMIM][DCA]/CuBTC and [BMIM][DBP]/CuBTC at 25 °C. For both composites, uptakes for all three gases are lower than those of pristine CuBTC [67] at all pressure points. Fig. S8(a) illustrates the experimental CO_2/CH_4, CO_2/N_2, and CH_4/N_2 selectivities of these new composites compared to those of the pristine CuBTC. Data show that both composites offer improved gas separation performance especially at low pressures, consistent with the previous reports [32,36,65,67].

Results of GCMC simulations for [BMIM][DCA]/CuBTC and [BMIM][DBP]/CuBTC composites were scaled using the same function as described above and in Table S15. Fig. 5(a) shows the good agreement between experiments and simulations. CO_2, CH_4, and N_2 uptakes were estimated well by the scaled GCMC simulations leading to R^2 values of 0.951, 0.897, and 0.964, respectively, while the raw GCMC simulation results have the corresponding R^2 values of 0.888, 0.873, and 0.805, respectively. Predicted ideal CO_2/CH_4, CO_2/N_2, and CH_4/N_2 selectivities of [BMIM][DCA]/CuBTC and [BMIM][DBP]/CuBTC were also in a reasonable agreement with the experimental selectivities as shown in Fig. S9. For example, experimental CO_2/N_2 selectivities vary between 4.5 and 16 at 0.5–10 bar, whereas simulations predicted these values as between 4.3 and 14.7. The experimental values for the ideal CO_2/CH_4 selectivity were between 1.4 and 3.5 at the same pressure range and the simulations estimated this selectivity as between 2 and 3.6.

We finally discuss the validity of the assumptions used to predict the gas adsorption properties of IL/CuBTC composites in this work. We considered CuBTC as a perfect crystal without defects in our molecular simulations. CuBTC we used in the experiments may have defects which may explain the overestimation of experimental gas uptake results by the GCMC simulations. Atomic positions of ILs in CuBTC were predicted with MD simulations in this work to save computational time in calculating the positions of 12 to 20 IL molecules inside a unit cell of MOF having 624 atoms but this is a rough estimation and quantum chemical/mechanical calculations are required for more accurate positions of ILs incorporated into MOFs. Finally, we used generic force fields which do not consider the specific chemical interactions [78,82–84] between IL and CuBTC, but previous experimental studies [32,36,65] suggested that IL incorporation may be changing not only the structure of the ILs, but also the electronic structure of the gas adsorption sites in MOFs. We attempted to use a generic force field to enable the transferability of our computational approach to various IL/MOF composites for high-throughput computational screening. Overall, these assumptions allowed us to provide an efficient computational approach, validated by experiments, which can quickly estimate the gas adsorption behavior in IL/CuBTC composites at a minimal computational expense, opening up opportunities for high-throughput screening studies on these novel materials.

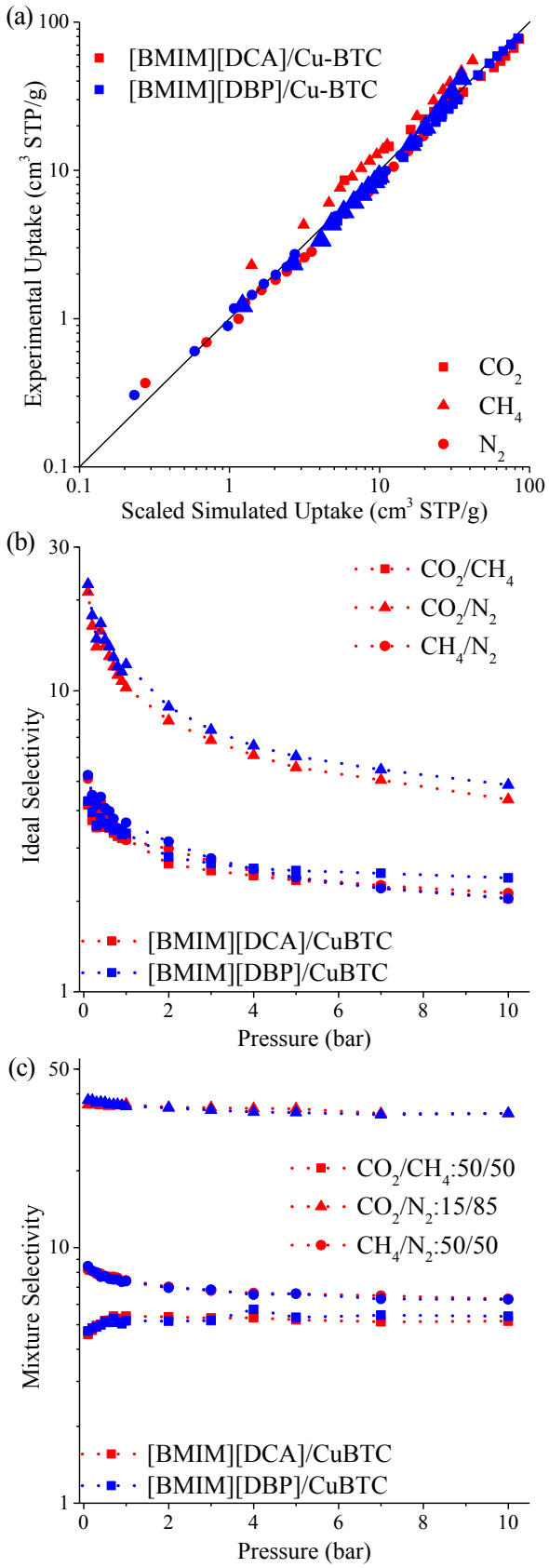


Fig. 5. (a) Comparison of scaled simulation results and experimental uptakes for [BMIM][DCA]/CuBTC and [BMIM][DBP]/CuBTC composites, (b) ideal and (c) mixture selectivities of two composites calculated from GCMC simulations. The first component in the label indicates the selected one over the other.

3.3. Gas mixture separation performances of IL/CuBTC composites

We also performed GCMC simulations considering CO_2/CH_4:50/50, CO_2/N_2:15/85, and CH_4/N_2:50/50 mixtures, which have industrial and environmental significance, at 0.1–10 bar to provide a more realistic gas separation performance analysis for all nine IL/CuBTC composites considered in this study. Fig. 5(b) and (c) demonstrate the ideal and mixture selectivities of [BMIM][DCA]/CuBTC and [BMIM][DBP]/CuBTC computed from GCMC simulations, respectively. Fig. S8(a) and (b) also show the experimental CO_2/CH_4, CO_2/N_2, and CH_4/N_2 selectivities and the corresponding mixture selectivities calculated by using the Ideal Adsorbed Solution Theory (IAST) [87]. Dual-site Langmuir fits were shown in Fig. S10 with their corresponding parameters listed in Table S16. Mixture selectivities in both cases were found to be higher than the ideal selectivities as expected because of the competition between the gas molecules for the same adsorption sites [88–91]. Ideal selectivities of the two new composites were computed to vary between 2.1–4.3 for CO_2/CH_4 and 4.3–22.6 for CO_2/N_2 in a pressure range of 0.1–10 bar, while they were between 3 and 4.1 and 7.7–15.4, respectively, for pristine CuBTC. As we showed in our previous studies [32,36,65], ILs act as additional interaction sites for adsorbate molecules at low pressures. Increase in CO_2 uptake because of the presence of these additional adsorption sites is higher than that of CH_4 and N_2, which leads to an increase in CO_2/CH_4 and CO_2/N_2 selectivities of composites at low pressures. However, at high pressures, available pore space for gas species becomes more dominant than the intermolecular interactions in determining the gas uptake performance, and thus, the selectivities decrease.

The comparison of mixture selectivities of all nine IL/CuBTC composites that we examined in this work with those of pristine CuBTC is given in Fig. S11. CO_2/CH_4:50/50, CO_2/N_2:15/85, and CH_4/N_2:50/50 mixture selectivities of all composites are higher than those of pristine CuBTC at all pressures except between 7 and 10 bar for CO_2/CH_4. At 0.1 bar, mixture selectivities of IL/CuBTC composites vary between 4.1–6.1, 31.5–44.7, and 6.5–8.5 for CO_2/CH_4, CO_2/N_2, and CH_4/N_2, respectively, while pristine CuBTC has a selectivity of 3.4, 15.7, and 4.9 for CO_2/CH_4, CO_2/N_2, and CH_4/N_2, respectively. These results suggest that IL/CuBTC composites that we examined in this work have a strong potential in separation of gas mixtures, especially for CO_2 separation from natural gas and flue gas. Using this computational approach, promising IL/MOF composites offering high selectivity for a desired gas separation can be identified among many possible candidates and the experimental efforts can then be focused on the synthesis and testing of these promising candidates.

3.4. Gas diffusion in IL/CuBTC composites

We so far examined the gas adsorption in IL/CuBTC composites. Kinetic properties of gases inside the pores of an adsorbent material are also important because slow diffusion due to the strong host-guest interactions can be a bottleneck in the adsorption processes [92]. To have an understanding on the gas transport inside the IL/CuBTC composites, MD simulations were performed and self-diffusivities of gases (D^0) in each IL/CuBTC composite were computed at infinite dilution. We specifically examined D^0 values in three cases to assess the effects of interactions between adsorbates and CuBTC and the ones between adsorbates and ILs: (i) only IL-gas interactions were considered, (ii) only CuBTC-gas interactions were considered, and (iii) both IL-gas and CuBTC-gas interactions were considered. Fig. 6 shows that D^0 of CO_2 is the lowest in all composites, 1.05×10^{-6}–1.34×10^{-5} cm^2/s, followed by CH_4 and N_2. This is expected as CO_2 has stronger interactions with the composite than CH_4 and N_2 have, leading to higher uptakes under the same conditions. Because of its stronger adsorption, it diffuses slower than the other gas components. D^0 values range between 1.21×10^{-6}–1.45×10^{-5} cm^2/s and 3.3×10^{-6}–3.76×10^{-5} cm^2/s for CH_4 and N_2, respectively. According to results presented in

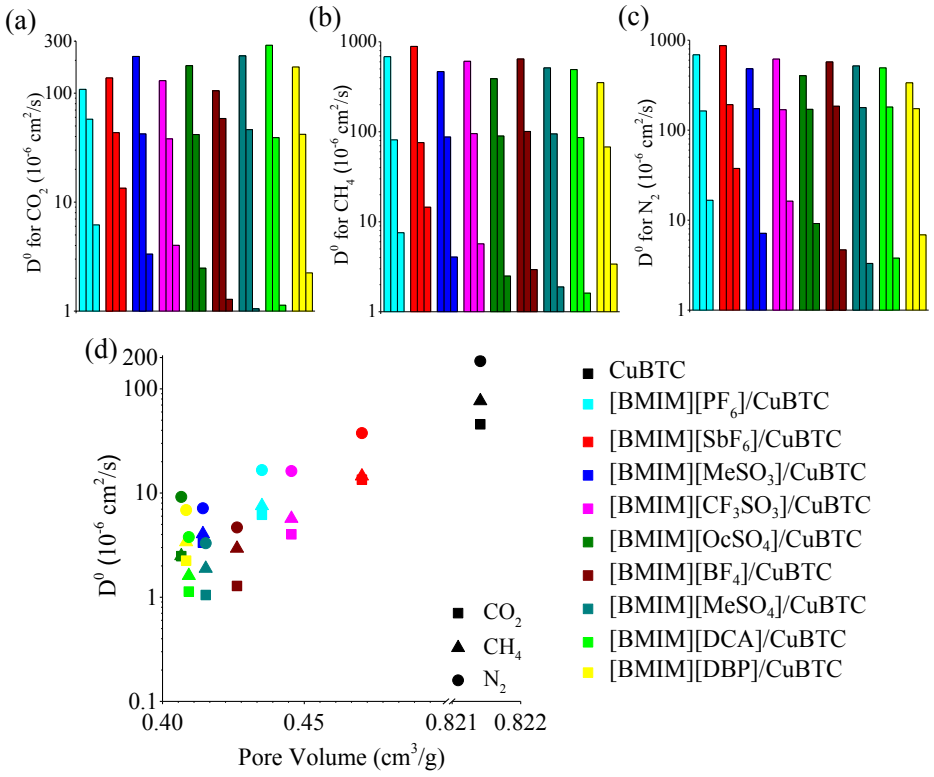


Fig. 6. D^0 values for (a) CO_2, (b) CH_4, and (c) N_2 in IL/CuBTC composites. For (a-c), IL-gas (CuBTC-gas) interactions are considered in the first (second) column. All interactions are considered in the third column. (d) Variation of D^0 values of CO_2, CH_4, and N_2 with respect to pore volume of IL/CuBTC composites and pristine CuBTC.

Fig. 6(a-c), D^0 values of all gases are the highest in case (i) than the ones in case (ii) for all IL/MOF composites, indicating that IL-gas interactions are weaker than the CuBTC-gas interactions because of the significantly larger number of interaction sites in CuBTC compared to IL molecules. Once both interactions were taken into account as in the case of (iii), gas molecules are strongly adsorbed and diffusivities become the lowest. Fig. 6(d) shows that D^0 values of gases in all IL/CuBTC composites are lower than those of pristine CuBTC, since IL molecules incorporated inside the pores of CuBTC decrease the pore volume of the material and hinder the gas mobility inside the cages. Among the IL/MOF composites we examined, [BMIM][SbF_6]/CuBTC has the highest gas diffusivities as it has the highest pore volume. We note that several factors other than the pore volume such as different chemical and physical properties of the anion of ILs may lead to differences in molecular interactions between gas molecules and IL molecules, which can be a major factor in determining the gas diffusivity [93,94].

Finally, we compared our simulated self-diffusion coefficients of gases in pristine CuBTC and IL/CuBTC composites with other available experimental and simulation studies. Experimental self-diffusion coefficient of CO_2 in CuBTC was reported as 1.7×10^{-5} cm^2/s at 0.5 vol% gas phase concentration of CO_2 in He at 1 bar at room temperature [95]. Schlayer et al. [96] measured self-diffusion coefficient of CH_4 in commercial CuBTC as 5.8×10^{-5} cm^2/s for 15 mg of CH_4/g of CuBTC at room temperature. Gutiérrez-Sevillano et al. [97] simulated CO_2/CH_4:50/50 mixture in pristine CuBTC and calculated diffusion coefficients of CH_4 and CO_2 at 0.1 bar at room temperature as 1.2×10^{-4} and 4×10^{-5} cm^2/s, respectively, without changing much with composition of the mixture. Our simulated self-diffusion coefficients for CH_4 and CO_2 were 7.7×10^{-5} and 4.6×10^{-5} cm^2/s, respectively, for pristine CuBTC at infinite dilution and these values were found to be consistent with the literature values listed above. Vicent-Luna et al. [47] calculated diffusion coefficients for CO_2 and CH_4 for [EMIM][SCN] incorporated IRMOF-1, MIL-47, MOF-1, and HMOF-1 at 1 bar at room temperature. The self-diffusion coefficients of CH_4 and CO_2 were reported to be between 5×10^{-6}–10^{-5} cm^2/s and 10^{-6}–7×10^{-6} cm^2/s, respectively, in 25 vol% IL incorporated MIL-47, 40 vol% IL incorporated MOF-1, and 35 vol% IL incorporated HMOF-1, which have similar pore volumes (0.41–0.48 cm^3/g) with the composites we studied in this work. Corresponding values were found to vary between 1.2×10^{-6}–1.5×10^{-5} cm^2/s for CH_4 and 10^{-6}–1.3×10^{-5} cm^2/s for CO_2 at infinite dilution in this study. We note that one may expect higher rate of gas transport at infinite dilution but the similarities of diffusivities between the reported work and ours can be explained with the longer chain of $[BMIM]^+$ than $[EMIM]^+$ and larger anions that we studied than linear $[SCN]^-$, both hinder the gas transport inside the cages.

4. Conclusions

Here, we proposed a computational methodology to predict CO_2, CH_4, and N_2 uptakes and CO_2/CH_4, CO_2/N_2, and CH_4/N_2 selectivities of IL/CuBTC composites, in which ILs are composed of $[BMIM]^+$ cation with different type of anions. We performed GCMC simulations on seven different IL/CuBTC composites, which were previously synthesized, and compared their simulated gas uptakes with the experimentally measured data. Two different generic force fields, UFF and Dreiding, were used to represent the IL/MOF composites and the one better representing the experimental gas uptake data (Dreiding) was chosen. We then offered a pressure dependent scaling factor to improve the agreement between simulations and experiments for the gas uptakes of IL/MOF composites. Motivated from the good agreement between experiments and simulations, we applied the same molecular simulation method to estimate the gas adsorption and separation performances of two new IL/CuBTC composites, which have not been synthesized before. These composites were synthesized, characterized, and their CO_2, CH_4, and N_2 uptakes were measured and compared with the predictions of molecular simulations. Results showed that the computational method that we validated on seven different IL/CuBTC composites can be used to efficiently and accurately predict the gas uptakes and selectivities of new IL/CuBTC composites, indicating transferability of the computational approach to different types of IL-incorporated CuBTC samples. We also performed GCMC simulations to provide a

more realistic performance of nine different IL/CuBTC composites for separation of gas mixtures. Results showed that CO_2/CH_4:50/50, CO_2/N_2:15/85, and CH_4/N_2:50/50 selectivities of all IL/CuBTC composites are higher than selectivities of pristine CuBTC from 0.1 to 7 bar. These results highlight the fact that IL-incorporated CuBTC composites have a strong potential for CO_2 separation from natural gas and flue gas mixtures. The computational approach that we used in this work can be expanded to other families of MOFs and ILs for high-throughput screening of IL/MOF composites to identify the promising materials which might offer extraordinarily high CO_2 selectivities.

Acknowledgments

S.K. acknowledges ERC-2017-Starting Grant. This research has received funding from the European Research Council (ERC) under the European Union's Horizon 2020 research and innovation programme (ERC-2017-Starting Grant, grant agreement No 756489-COSMOS). This work is also supported by the Scientific and Technological Research Council of Turkey (TUBITAK) under 1001-Scientific and Technological Research Projects Funding Program (project number: 114R093) and by Koç University Seed Fund Program. Support provided by the KUTEM (Koç University TÜPRAŞ Energy Center) is gratefully acknowledged. A.U. acknowledges the TUBA-GEBIP Award. Authors thank Koç University Surface Science and Technology Center (KUYTAM) for providing help with the sample characterization. Authors would like to thank TARLA for the collaborative research support.

Appendix A. Supplementary data

Supplementary data to this article can be found online at https://doi.org/10.1016/j.cej.2019.05.113.

References

[1] J.G. Vitillo, B. Smit, L. Gagliardi, Introduction: Carbon capture and separation, Chem. Rev. 117 (2017) 9521–9523.
[2] A. Schoedel, Z. Ji, O.M. Yaghi, The role of metal-organic frameworks in a carbon neutral energy cycle, Nat. Energy 1 (2016) 16034.
[3] Y. Belmabkhout, V. Guillerm, M. Eddaoudi, Low concentration CO_2 capture using physical adsorbents: are metal–organic frameworks becoming the new benchmark materials? Chem. Eng. J. 296 (2016) 386–397.
[4] M. Oschatz, M. Antonietti, A search for selectivity to enable CO_2 capture with porous adsorbents, Energy Environ. Sci. 11 (2018) 57–70.
[5] M.R. Raupach, G. Marland, P. Ciais, C. Le Quere, J.G. Canadell, G. Klepper, C.B. Field, Global and regional drivers of accelerating CO_2 emissions, Proc. Natl. Acad. Sci. U.S.A. 104 (2007) 10288–10293.
[6] S. Cavenati, C.A. Grande, A.E. Rodrigues, Removal of carbon dioxide from natural gas by vacuum pressure swing adsorption, Energy Fuels 20 (2006) 2648–2659.
[7] D.Y.C. Leung, G. Caramanna, M.M. Maroto-Valer, An overview of current status of carbon dioxide capture and storage technologies, Renew. Sust. Energy Rev. 39 (2014) 426–443.
[8] J. Park, M. Jung, H. Jang, K. Lee, N.F. Attia, H. Oh, A facile synthesis of tool of nanoporous carbon for promising H_2, CO_2 and CH_4 sorption capacity and selective gas adsorption, J. Mater. Chem. A 6 (2018) 23087–23100.
[9] Y. Jiang, J. Ling, P. Xiao, Y. He, Q. Zhao, Z. Chu, Y. Liu, Z. Li, P.A. Webley, Simultaneous biogas purification and CO_2 capture by vacuum swing adsorption using zeolite NaUSY, Chem. Eng. J. 334 (2018) 2593–2602.
[10] N. Kosinov, C. Auffret, C. Gucuyener, B.M. Szyja, J. Gascon, F. Kapteijn, E.J.M. Hensen, High flux high-silica SSZ-13 membrane for CO_2 separation, J. Mater. Chem. A 2 (2014) 13083–13092.
[11] Y. Jiao, Y. Zheng, S.C. Smith, A. Du, Z. Zhu, Electrocatalytically switchable CO_2 capture: First principle computational exploration of carbon nanotubes with pyridinic nitrogen, ChemSusChem 7 (2014) 435–441.
[12] A.K. Adhikari, K.S. Lin, Improving CO_2 adsorption capacities and CO_2/N_2 separation efficiencies of MOF-74(Ni, Co) by doping palladium-containing activated carbon, Chem. Eng. J. 284 (2016) 1348–1360.
[13] S. Keskin, D.S. Sholl, Selecting metal organic frameworks as enabling materials in mixed matrix membranes for high efficiency natural gas purification, Energy Environ. Sci. 3 (2010) 343–351.
[14] A. Uzun, S. Keskin, Site characteristics in metal organic frameworks for gas adsorption, Prog. Surf. Sci. 89 (2014) 56–79.
[15] H. Furukawa, K.E. Cordava, M. O'keeffe, O.M. Yaghi, The chemistry and applications of metal-organic frameworks, Science 341 (2013) 974.
[16] W. Meng, Y. Zeng, Z. Liang, W. Guo, C. Zhi, Y. Wu, R. Zhong, C. Qu, R. Zou, Tuning expanded pores in metal-organic frameworks for selective capture and catalytic conversion of carbon dioxide, ChemSusChem 11 (2018) 3751–3757.
[17] C. Sun, C. Qin, C. Wang, Z. Su, S. Wang, X. Wang, G. Yang, K. Shao, Y. Lan, E. Wang, Chiral nanoporous metal-organic frameworks with high porosity as materials for drug delivery, Adv. Mater. 23 (2011) 5629–5632.
[18] S. Bureekaew, S. Horike, M. Higuchi, M. Mizuno, T. Kawamura, D. Tanaka, N. Yanai, S. Kitagawa, One-dimensional imidazole aggregate in aluminium porous coordination polymers with high proton conductivity, Nat. Mater. 8 (2009) 831–836.
[19] J. Jiang, H. Furukawa, Y. Zhang, O.M. Yaghi, High methane storage working capacity in metal-organic frameworks with acrylate links, J. Am. Chem. Soc. 138 (2016) 10244–10251.
[20] S. Keskin, T.M. van Heest, D.S. Sholl, Can metal-organic framework materials play a useful role in large-scale carbon dioxide separations? ChemSusChem 3 (2010) 879–891.
[21] A.O. Yazaydin, R.Q. Snurr, T. Park, K. Koh, J. Liu, M.D. LeVan, A.I. Benin, P. Jakubczak, M. Lanuza, D.B. Galloway, J.J. Low, R.R. Willis, Screening of metal-organic frameworks for carbon dioxide capture from flue gas using a combined experimental and modeling approach, J. Am. Chem. Soc. 131 (2009) 18198–18199.
[22] J. Li, Y. Tao, Q. Yu, X. Bu, H. Sakamoto, S. Kitigawa, Selective gas adsorption and unique structural topology of a highly stable guest-free zeolite-type MOF material with N-rich chiral open channels, Chem. Eur. J. 14 (2008) 2771–2776.
[23] Z. Lei, B. Chen, Y. Koo, D.R. MacFarlane, Introduction: Ionic liquids, Chem. Rev. 117 (2017) 6633–6635.
[24] K.N. Marsh, J.A. Boxall, R. Lichtenthaler, Room temperature ionic liquids and their mixtures-a review, Fluid Phase Equilib. 219 (2004) 93–98.
[25] A. Noda, K. Hayamizu, M. Watanabe, Pulse-gradient spin-echo ^1H and ^{19}F NMR ionic diffusion coefficient, viscosity, and ionic conductivity of non-chloroaluminate room-temperature ionic liquids, J. Phys. Chem. B 105 (2001) 4603–4610.
[26] J. Liao, P. Wu, W. Huang, Ionic liquid as solvent for the synthesis and crystallization of a coordination polymer: (EMI)[Cd(BTC)] (EMI = 1-Ethyl-3-methylimidazolium, BTC = 1,3,5-Benzenetricarboxylate), Cryst Growth Des. 6 (2006) 1062–1063.
[27] D.N. Dybtsev, H. Chun, K. Kim, Three-dimensional metal–organic framework with (3,4)-connected net, synthesized from an ionic liquid medium, Chem. Commun. 14 (2004) 1594–1595.
[28] X. Sang, J. Zhang, J. Xiang, J. Cui, L. Zheng, J. Zhang, Z. Wu, Z. Li, G. Mo, Y. Xu, J. Song, C. Liu, X. Tan, T. Luo, B. Zhang, B. Han, Ionic liquid accelerates the crystallization of Zr-based metal-organic frameworks, Nat. Commun. 8 (2017) 175.
[29] A. Jalal, A. Uzun, An ordinary nickel catalyst becomes completely selective for partial hydrogenation of 1,3-butadiene when coated with tributyl(methyl)phosphonium methyl sulfate, Appl. Catal., A 562 (2018) 321–326.
[30] P. Sharma, S. Do Park, K.T. Park, S.C. Nam, S.K. Jeong, Y. Il Yoon, I.H. Baek, Solubility of carbon dioxide in amine-functionalized ionic liquids: role of the anions, Chem. Eng. J. 193–194 (2012) 267–275.
[31] G. Cui, J. Zheng, X. Luo, W. Lin, F. Ding, H. Li, C. Wang, Tuning amino-functionalized ionic liquids for improved SO_2 capture, Angew. Chem. – Int. Ed. 52 (2013) 10620–10624.
[32] F.P. Kinik, C. Altintas, V. Balci, B. Koyuturk, A. Uzun, S. Keskin, [BMIM][PF_6] incorporation doubles CO_2 selectivity of ZIF-8: elucidation of interactions and their consequences on performance, ACS Appl. Mater. Interfaces 8 (2016) 30992–31005.
[33] M. Zeeshan, V. Nozari, M.B. Yagci, T. Isik, U. Unal, V. Ortalan, S. Keskin, A. Uzun, Core–shell type ionic liquid/metal organic framework composite: an exceptionally high CO_2/CH_4 selectivity, J. Am. Chem. Soc. 140 (2018) 10113–10116.
[34] Y. Ban, Z. Li, Y. Li, Y. Peng, H. Jin, W. Jiao, A. Guo, P. Wang, Q. Yang, C. Zhong, W. Yang, Confinement of ionic liquids in nanocages: tailoring the molecular sieving properties of ZIF-8 for membrane-based CO_2 capture, Angew. Chem. – Int. Ed. 54 (2015) 15483–15487.
[35] H.M.A. Hassan, M.A. Betiha, S.K. Mohamed, E.A. El-Sharkawy, E.A. Ahmed, Stable and recyclable MIL-101(Cr)-Ionic liquid based hybrid nanomaterials as heterogeneous catalyst, J. Mol. Liq. 236 (2017) 385-384.
[36] B. Koyuturk, C. Altintas, F.P. Kinik, S. Keskin, A. Uzun, Improving gas separation performance of ZIF-8 by [BMIM][BF_4] incorporation: Interactions and their consequences on performance, J. Phys. Chem C 121 (2017) 10370–10381.
[37] M. Mohamedali, H. Ibrahim, A. Henni, Incorporation of acetate-based ionic liquids into a zeolitic imidazolate framework (ZIF-8) as efficient sorbents for carbon dioxide capture, Chem. Eng. J. 334 (2018) 817–828.
[38] F.P. Kinik, A. Uzun, S. Keskin, Ionic liquid/metal-organic framework composites: from synthesis to applications, ChemSusChem 10 (2017) 2842–2863.
[39] C. Altintas, G. Avci, H. Daglar, A. Nemati Vesali Azar, S. Velioglu, I. Erucar, S. Keskin, Database for CO_2 separation performances of MOFs based on computational materials screening, ACS Appl. Mater. Interfaces 10 (2018) 17257–17268.
[40] W. Wei, K. Zhang, Z. Qiao, J. Jiang, Functional UiO-66 for the removal of sulfur-containing compounds in gas and liquid mixtures: a molecular simulation study, Chem. Eng. J. 356 (2019) 737–745.
[41] H. Xing, X. Zhao, Q. Yang, B. Su, Z. Bao, Y. Yang, Q. Ren, Molecular dynamics simulation study on the absorption of ethylene and acetylene in ionic liquids, Ind. Eng. Chem. Res. 52 (2013) 9308–9316.
[42] Y. Chen, Z. Hu, K.M. Gupta, J. Jiang, Ionic liquid/metal–organic framework composite for CO_2 capture: a computational investigation, J. Phys. Chem. C 115 (2011) 21736–21742.
[43] J.M. Vicent-Luna, J.J. Gutierrez-Sevillano, J.A. Anta, S. Calero, Effect of room-temperature ionic liquids on CO_2 separation by a Cu-BTC metal-organic framework, J. Phys. Chem. C 117 (2013) 20762–20768.
[44] Z. Li, Y. Xiao, W. Xue, Q. Yang, C. Zhong, Ionic Liquid/Metal–organic framework composites for H_2S removal from natural gas: a computational exploration, J. Phys. Chem. C 119 (2015) 3674–3683.
[45] W. Xue, Z. Li, H. Huang, Q. Yang, D. Liu, Q. Xu, C. Zhong, Effects of ionic liquid

dispersion in metal-organic frameworks and covalent organic frameworks on CO_2 capture: a computational study, Chem. Eng. Sci. 140 (2016) 1–9.
[46] J.M. Vicent-Luna, A. Luna-Triguero, S. Calero, Storage and separation of carbon dioxide and methane in hydrated covalent organic frameworks, J. Phys. Chem. C 120 (2016) 23756–23762.
[47] J.M. Vicent-Luna, J.J. Gutierrez-Sevillano, S. Hamad, J. Anta, S. Calero, Role of ionic liquid $[EMIM]^+[SCN]^-$ in the adsorption and diffusion of gases in metal–organic frameworks, ACS Appl. Mater. Interfaces 10 (2018) 29694–29704.
[48] K.M. Gupta, Y. Chen, Z. Hu, J. Jiang, Metal–organic framework supported ionic liquid membranes for CO_2 capture: anion effects, Phys. Chem. Chem. Phys. 14 (2012) 5785–5794.
[49] K.M. Gupta, Y. Chen, J. Jiang, Ionic liquid membranes supported by hydrophobic and hydrophilic metal–organic frameworks for CO_2 capture, J. Phys. Chem. C 117 (2013) 5792–7699.
[50] M.J. Frisch, G.W. Trucks, H.B. Schlegel, G.E. Scuseria, M.A. Robb, J.R. Cheeseman, G. Scalmani, V. Barone, G.A. Petersson, H. Nakatsuji, X. Li, M. Caricato, A. Marenich, J. Bloino, B.G. Janesko, R. Gomperts, B. Mennucci, H.P. Hratchian, J.V. Ortiz, A.F. Izmaylov, J.L. Sonnenberg, D. Williams-Young, F. Ding, F. Lipparini, F. Egidi, J. Goings, B. Peng, A. Petrone, T. Henderson, D. Ranasinghe, V.G. Zakrzewski, J. Gao, N. Rega, G. Zheng, W. Liang, M. Hada, M. Ehara, K. Toyota, R. Fukuda, J. Hasegawa, M. Ishida, T. Nakajima, Y. Honda, O. Kitao, H. Nakai, T. Vreven, K. Throssell, J.A. Montgomery Jr., J.E. Peralta, F. Ogliaro, M. Bearpark, J.J. Heyd, E. Brothers, K.N. Kudin, V.N. Staroverov, T. Keith, R. Kobayashi, J. Normand, K. Raghavachari, A. Rendell, J.C. Burant, S.S. Iyengar, J. Tomasi, M. Cossi, J.M. Millam, M. Klene, C. Adamo, R. Cammi, J.W. Ochterski, R.L. Martin, K. Morokuma, O. Farkas, J.B. Foresman, D.J. Fox, Gaussian 09 (Revision A.02), Gaussian Inc., Wallingford CT, 2016.
[51] A.D. Becke, Density-functional thermochemistry. III. The role of exact exchange, J. Chem. Phys. 98 (1993) 5648–5652.
[52] C. Lee, W. Yang, R.G. Parr, Development of the Colve-Salvetti correlation-energy formula into a functional of electron density, Phys. Rev. B 37 (1988) 785–789.
[53] N. Godbout, D.R. Salahub, Optimization of gaussian-type basis sets for local spin density functional calculations. Part I. Boron through neon, optimization technique and validation, Can. J. Chem. 70 (1992) 560–571.
[54] J.P. Foster, F. Weinhold, Natural hybrid orbitals, J. Am. Chem. Soc. 102 (1980) 7211–7218.
[55] A.E. Reed, L.A. Curtiss, F. Weinhold, Intermolecular interactions from a natural bond orbital, donor-acceptor viewpoint, Chem. Rev. 88 (1988) 899–926.
[56] D. Dubbeldam, S. Calero, D.E. Ellis, R.Q. Snurr, RASPA: molecular simulation software for adsorption and diffusion in flexible nanoporous materials, Mol. Simul. 42 (2016) 81–101.
[57] A.K. Rappe, C.J. Casewit, K.S. Colwell, W.A. Goddard III, W.M. Skiff, UFF, a full periodic table force field for molecular mechanics and molecular dynamics simulations, J. Am. Chem. Soc. 114 (1992) 10024–10035.
[58] S.L. Mayo, B.D. Olafson, W.A. Goddard III, DREIDING: a generic force field for molecular simulations, J. Phys. Chem. 94 (1990) 8897–8909.
[59] J.J. Potoff, J.I. Siepmann, Vapor-liquid equilibria of mixtures containing alkanes, carbon dioxide, and nitrogen, AIChE J. 47 (2001) 1676–1682.
[60] D. Dubbeldam, S. Calero, T.J.H. Vlugt, R. Krishna, T.L.M. Maesen, B. Smit, United atom force field for alkanes in nanoporous materials, J. Phys. Chem. B 108 (2004) 12301–12313.
[61] K. Makrodimitris, G.K. Papadopoulos, D.N. Theodorou, Prediction of permeation properties of CO_2 and N_2 through silicalite via molecular simulations, J. Phys. Chem. B 105 (2001) 777–788.
[62] L. Zhao, Q. Yang, Q. Ma, C. Zhong, J. Mi, D. Liu, A force field for dynamic Cu-BTC metal-organic framework, J. Mol. Model. 17 (2011) 227–234.
[63] T.F. Willems, C.H. Rycroft, M. Kazi, J.C. Meza, M. Haranczyk, Algorithms and tools for high-throughput geometry-based analysis of crystalline porous materials, Microporous Mesoporous Mater. 149 (2012) 134–141.
[64] D. Dubbeldam, R. Krishna, R.Q. Snurr, Method for analyzing structural changes of flexible metal-organic frameworks induced by adsorbates, J. Phys. Chem. C 113 (2009) 19317–19327.
[65] K.B. Sezginel, S. Keskin, A. Uzun, Tuning the gas separation performance of CuBTC by ionic liquid incorporation, Langmuir 32 (2016) 1139–1147.
[66] V. Nozari, S. Keskin, A. Uzun, Toward rational design of ionic liquid/metal–organic framework composites: effects of interionic interaction energy, ACS Omega 2 (2017) 6613–6618.
[67] V. Nozari, M. Zeeshan, S. Keskin, A. Uzun, Effect of methylation of ionic liquids on the gas separation performance of ionic liquid/metal–organic framework composites, CrystEngComm 20 (2018) 7137–7143.
[68] C.E. Wilmer, R.Q. Snurr, Towards rapid computational screening of metal-organic frameworks for carbon dioxide capture: calculation of framework charges via charge equilibration, Chem. Eng. J. 171 (2011) 775–781.
[69] S. Nose, A molecular dynamics method for simulations in the canonical ensemble, Mol. Phys. 52 (1984) 255–268.
[70] W.G. Hoover, Canonical dynamics: equilibrium phase-space distributions, Phys. Rev. A 31 (1985) 1695–1697.
[71] M. Babucci, C. Fang, J.E. Perez-Aguilar, A.S. Hoffman, A. Boubnov, E. Guan, S.R. Bare, B.C. Gates, A. Uzun, Controlling catalytic activity and selectivity for partial hydrogenation by tuning the environment around active sites in iridium complexes bonded to supports, Chem. Sci. (2019) Advance Article.
[72] J.R. Karra, K.S. Walton, Effect of open metal sites on adsorption of polar and nonpolar molecules in metal-organic framework Cu-BTC, Langmuir 24 (2008) 8620–8626.
[73] J.R. Karra, K.S. Walton, Molecular simulations and experimental studies of CO_2, CO, and N_2 adsorption in metal-organic frameworks, J. Phys. Chem. C 114 (2010) 15735–15740.
[74] H.S. Koh, M.K. Rana, A.G. Wong-Foy, D.J. Siegel, Predicting methane storage in open-metal-site metal–organic frameworks, J. Phys. Chem. C 119 (2015) 13451–13458.
[75] A.O. Yazaydin, A.I. Benin, S.A. Faheem, P. Jakubczak, J.J. Low, R.R. Willis, R.Q. Snurr, Enhanced CO_2 adsorption in metal-organic frameworks via occupation of open-metal sites by coordinated water molecules, Chem. Mater. 21 (2009) 1425–1430.
[76] C. Altintas, I. Erucar, S. Keskin, High-throughput computational screening of the metal organic framework database for CH_4/H_2 separations, ACS Appl. Mater. Interfaces 10 (2018) 3668–3679.
[77] D. Fairen-Jimenez, P. Lozano-Casal, T. Duren, Assessing generic force fields to describe adsorption on metal-organic frameworks, in: S. Kaskel, P. Llewellyn, F. Rodriguez-Reinoso, N.A. Seaton (Eds.), Characterisation of Porous Solids VIII, RSC Publishing, Cambridge, UK, 2009, pp. 80–87.
[78] C. Campbell, C.A. Ferreiro-Rangel, M. Fischer, J.R.B. Gomes, M. Jorge, A transferable model for adsorption in MOFs with unsaturated metal sites, J. Phys. Chem. C 121 (2017) 441–458.
[79] Y. Bae, K.L. Mulfort, H. Frost, P. Ryan, S. Punnathanam, L.J. Broadbelt, J.T. Hupp, R.Q. Snurr, Separation of CO_2 from CH_4 using mixed-ligand metal-organic frameworks, Langmuir 24 (2008) 8592–8598.
[80] S. Surble, F. Millange, C. Serre, T. Duren, M. Latroche, S. Bourrelly, P.L. Llewellyn, G. Ferey, Synthesis of MIL-102, a chromium carboxylate metal-organic framework, with gas sorption analysis, J. Am. Chem. Soc. 128 (2006) 14889–14896.
[81] D. Dubbeldam, H. Frost, K.S. Walton, R.Q. Snurr, Molecular simulation of adsorption sites of light gases in the metal-organic framework IRMOF-1, Fluid Phase Equilib. 261 (2007) 152–161.
[82] J. Perez-Pellitero, J. Amrouche, F.R. Siperstein, G. Pirngruber, C. Nieto-Draghi, G. Chaplais, A. Simon-Masseron, D. Bazer-Bachi, D. Peralta, N. Bats, Adsorption of CO_2, CH_4, and N_2 on zeolitic imidazolate frameworks: experiments and simulations, Chem. Eur. J. 16 (2010) 1560–1571.
[83] T. Sagara, J. Klassen, J. Ortony, E. Ganz, Binding energies of hydrogen molecules to isoreticular metal-organic framework materials, J. Chem. Phys. 123 (2005) 1–5.
[84] M. Tafipolsky, R. Schmid, Systematic first principles parameterization of force fields for metal-organic frameworks using a genetic algorithm approach, J. Phys. Chem. B 113 (2009) 1341–1351.
[85] C.Y. Penalber, Z. Grenoble, G.A. Baker, S. Baldelli, Surface characterization of imidazolium-based ionic liquids with cyano-functionalized anions at the gas–liquid interface using sum frequency generation spectroscopy, Phys. Chem. Chem. Phys. 14 (2012) 5122–5131.
[86] T.G. Levitskaia, J.M. Peterson, E.L. Campbell, A.J. Casella, D.R. Peterman, S.A. Bryan, Fourier transform infrared spectroscopy and multivariate analysis for online monitoring of dibutyl phosphate degradation product in tributyl phosphate/n-dodecane/nitric acid solvent, Ind. Eng. Chem. Res. 52 (2013) 17607–17617.
[87] S. Lee, J.H. Lee, J. Kim, User-friendly graphical user interface software for ideal adsorbed solution theory calculations, Korean J. Chem. Eng. 35 (2018) 214–221.
[88] K. Tan, S. Zuluaga, Q. Gong, Y. Gao, N. Nijem, J. Li, T. Thonhauser, Y.J. Chabal, Competitive coadsorption of CO_2 with H_2O, NH_3, SO_2, NO, NO_2, N_2, O_2, and CH_4 in M-MOF 74 (M = Mg Co, Ni): the role of hydrogen bonding, Chem. Mater. 27 (2015) 2203–2217.
[89] L. Joos, J.A. Swisher, B. Smit, Molecular simulation study of the competitive adsorption of H_2O and CO_2 in Zeolite 13X, Langmuir 29 (2013) 15936–15942.
[90] J. Liu, Y. Wang, A.I. Benin, P. Jakubczak, R.R. Willis, M.D. LeVan, CO_2/H_2O adsorption equilibrium and rates on metal-organic frameworks: HKUST-1 and Ni/DOBDC, Langmuir 26 (2010) 14301–14307.
[91] Z. Zhang, Z. Li, J. Li, Computational study of adsorption and separation of CO_2, CH_4, and N_2 by an rht-type metal–organic framework, Langmuir 28 (2012) 12122–12133.
[92] P. Canepa, N. Nijem, Y.J. Chabal, T. Thonhauser, Diffusion of small molecules in metal organic framework materials, Phys. Rev. Lett. 110 (2013) 1–5.
[93] M. Gonzalez-Miquel, J. Bedia, C. Abrusci, J. Palomar, F. Rodriguez, Anion effects on kinetics and thermodynamics of CO_2 absorption in ionic liquids, J. Phys. Chem. B 117 (2013) 3398–3406.
[94] Y. Hu, Z. Liu, C. Xu, X. Zhang, The molecular characteristics dominating the solubility of gases in ionic liquids, Chem. Soc. Rev. 40 (2011) 3802–3823.
[95] T.M. Tovar, J. Zhao, W.T. Nunn, H.F. Barton, G.W. Peterson, G.N. Parsons, M.D. LeVan, Diffusion of CO_2 in large crystals of Cu-BTC MOF, J. Am. Chem. Soc. 138 (2016) 11449–11452.
[96] S. Schlayer, A.-K. Pusch, F. Pielenz, S. Beckert, M. Peksa, C. Horch, L. Moschkowitz, W.-D. Einicke, F. Stallmach, X-nuclei NMR self-diffusion studies in mesoporous silica foam and microporous MOF CuBTC, Materials 5 (2012) 617–633.
[97] J.J. Gutierrez-Sevillano, A. Caro-Perez, D. Dubbeldam, S. Calero, Molecular simulation investigation into the performance of Cu–BTC metal–organic frameworks for carbon dioxide–methane separations, Phys. Chem. Chem. Phys. 13 (2011) 20453–20460.